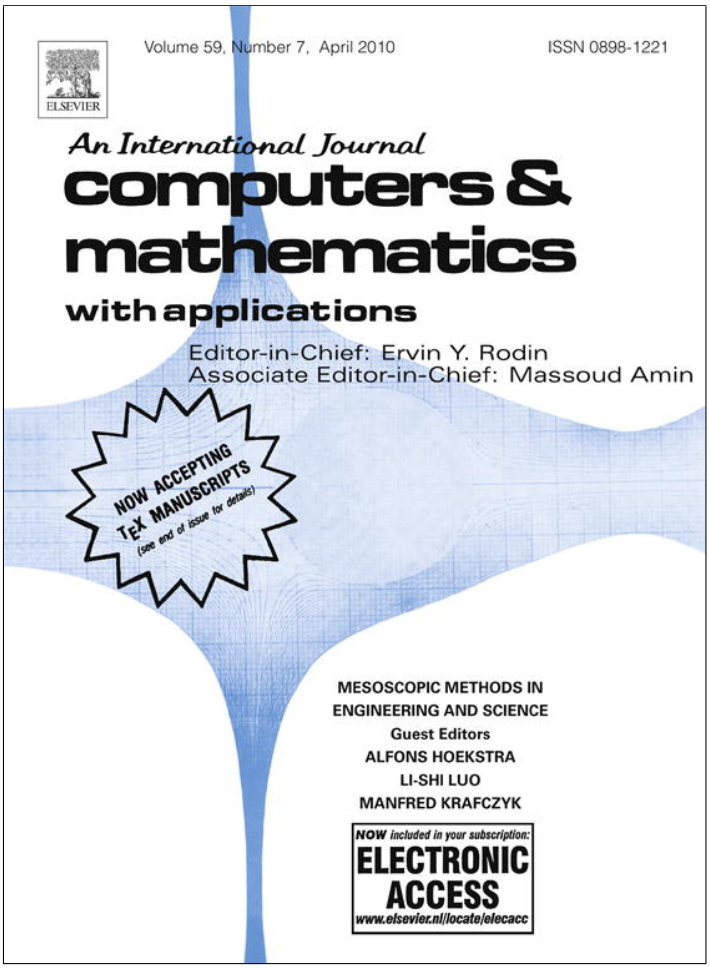

Computers and Mathematics with Applications 59 (2010) 2326–2339

Contents lists available at ScienceDirect

Computers and Mathematics with Applications

journal homepage: www.elsevier.com/locate/camwa

Prediction of traveling front behavior in a lattice-gas cellular automaton model for tumor invasion

H. Hatzikirou [a,*], L. Brusch [a], C. Schaller [c], M. Simon [b], A. Deutsch [a]

[a] Center for Information Services and High Performance Computing, Technische Universität Dresden, Nöthnitzerstr. 46, 01069 Dresden, Germany

[b] Department of Neurosurgery, University of Bonn Medical Center, Sigmund-Freud-Str. 25, 53105 Bonn, Germany

[c] Department of Neurosurgery, University Hospital of Geneva, 24 Rue Micheli-du-Crest, 1211 Geneva, Switzerland

ARTICLE INFO

Keywords:
Tumor invasion
Lattice-gas cellular automata
Lattice Boltzmann equation
Traveling fronts
Cut-off mean-field approximation

ABSTRACT

Cancer invasion is the process of cells detaching from a primary tumor and infiltrating the healthy tissue. Cancer invasion has been recognized as a complex system, since a tumor's invasive behavior emerges from the combined effect of tumor cell proliferation, tumor cell migration and cell–microenvironment interactions. Cellular automata (CA) provide simple models of self-organizing complex systems in which collective behavior can emerge out of an ensemble of many interacting "simple" components. Here, we introduce a lattice-gas cellular automaton (LGCA) model of tumor cell proliferation, necrosis and tumor cell migration. The impact of the tumor environment on tumor cells has been investigated in a previous study. Our analysis aims at predicting the velocity of the traveling invasion front, which depends upon fluctuations that arise from the motion of the discrete cells at the front. We find an excellent agreement between the velocities measured in simulations of the LGCA and an analytical estimate derived in the cut-off mean-field approximation via the discrete Lattice Boltzmann equation and its linearization. In particular, we predict the front velocity to scale with the square root of the product of probabilities for mitosis and the migration coefficient. Finally, we calculate the width of the traveling front which is found to be proportional to the front velocity.

1. Introduction

Cancer describes a group of genetic and epigenetic diseases, characterized by uncontrolled growth of cells, leading to a variety of pathological consequences and frequently death. Cancer has long been recognized as an evolutionary disease [1]. Cancer progression can be depicted as a sequence of traits or phenotypes that cells have to acquire if a neoplasm (benign tumor) is to become an invasive and malignant cancer. A phenotype refers to any kind of observed morphology, function or behavior of a living cell. Hanahan and Weinberg [2] have identified six cancer cell phenotypes: unlimited proliferative potential, environmental independence for growth, evasion of apoptosis, angiogenesis, invasion and metastasis.

In this article, we concentrate on the behavior of the invasive phenotype. The progression of a benign tumor with limited growth to a tumor that is invasive and potentially metastatic is the major cause of poor clinical outcome in cancer patients, in terms of therapy and prognosis. Understanding tumor invasion could potentially lead to the design of novel therapeutical strategies. However, despite the immense amounts of funds invested in cancer research, the dynamics that govern tumor invasiveness *in vivo* remain poorly understood.

* Corresponding author.
E-mail address: haralambos.hatzikirou@tu-dresden.de (H. Hatzikirou).

0898-1221/$ – see front matter © 2009 Elsevier Ltd. All rights reserved.
doi:10.1016/j.camwa.2009.08.041

Biomedically, invasion involves the following tumor cell *processes*:

- tumor cell migration, which is a result of down-regulation of cadherins[1] and corresponding loss of cell–cell adhesion,
- tumor cell–extracellular matrix (ECM)[2] interactions, such as cell-ECM adhesion, and ECM degradation/remodeling, by means of proteolysis. These processes allow for the penetration of the migrating tumor cells into host tissue barriers, such as basement and interstitial stroma [3], and
- tumor cell proliferation.

Tumor invasion facilitates the emergence of metastases, i.e. the spread of cancer cells to another part of the body and the formation of secondary tumors. It is obvious that tumor invasion comprises a central aspect in cancer progression. However, invasive phenomena occur not only in pathological cases of malignant tumors but also during normal morphogenesis and wound healing. In this study, we focus on the impact of tumor cell migration and proliferation on invasive behavior. The effect of the tumor environment on tumor cells, and in particular on the migration of tumor cells, has been discussed in a previous study by the authors [4].

Several mathematical models have been proposed to describe the temporal or spatio-temporal dynamics of tumor proliferation and invasion. Much of the experimental data that exists has been modeled using purely time-dependent growth laws based on the assumption of either exponential or Gompertzian growth [5]. Additionally, the spatio-temporal evolution of a proliferative tumor cell population has been modeled as a behavior that emerges from local micro-interactions [6]. Deterministic reaction–diffusion models have been used to model the spatio-temporal growth of tumors, usually assuming that tumor growth is a wave propagation phenomenon [7–11] and is driven by random movement of malignant cells [12]. Swanson et al. [13] modeled proliferation and migration of brain tumors based on actual clinical data. Recently, innovative methods have been developed by employing a mathematical and computational model that describes tumor growth and invasion [14].

Whilst these models are able to capture the tumor structure at the tissue level they fail to describe the tumor at the cellular and the sub-cellular levels. Cellular automata (CA) models can provide such a micro-scale description and allow a more realistic stochastic approach at the cellular level. In particular, Hatzikirou et al. [15] present a detailed review of cellular automata of tumor invasion. We introduce a particular class of CA with a structure that allows for a feasible mathematical analysis, the so-called lattice-gas cellular automata (LGCA) [16,17]. In contrast to traditional cellular automata, LGCA allow for a straightforward and intuitive implementation of cell migration and interactions. LGCA have been recently used to study tumor growth [18], cell motion under the influence of a heterogeneous environment [4] and the investigation of brain tumor invasion [19].

In this paper we combine a detailed micro-scale model with an analysis of the corresponding macro-scale approximation. We describe a simple LCGA model of interacting tumor cells and "necrotic entities". LGCA provide a concrete framework to conduct analytical and numerical analysis [16,20,21]. By means of a mean-field approximation, we are able to derive a macroscopic partial differential equation (PDE) describing our system. This equation characterizes the spatio-temporal tumor expansion at the tissue level. Introducing a cut-off in the mean-field macroscopic description allows for a quantitative characterization of the traveling wavefront. We calculate analytically the front speed and we compare it with the values derived from simulations. This analysis enables us to estimate tumor spreading by known tumor cell features, such as cell motility and proliferation rate. Finally, we provide an analytical estimate of the front width and we demonstrate that it is proportional to the front speed.

2. Model definition

2.1. Prerequisites

We consider a lattice-gas cellular automaton defined on a two-dimensional regular lattice $\mathcal{L} = L_1 \times L_2 \in \mathbb{Z}^2$, where L_1, L_2 are the lattice dimensions. Let b denote the coordination number of the lattice, that is $b = 4$ for a square lattice. Cells move on the discrete lattice with discrete velocities, i.e. they hop at discrete time steps from a given node to a neighboring one, as determined by the cell velocity. The set of velocities for the square lattice as considered here, is represented by the two-dimensional channel velocity vectors

$$\mathbf{c}_1 = \begin{pmatrix} 1 \\ 0 \end{pmatrix}, \qquad \mathbf{c}_2 = \begin{pmatrix} 0 \\ 1 \end{pmatrix}, \qquad \mathbf{c}_3 = \begin{pmatrix} -1 \\ 0 \end{pmatrix}, \qquad \mathbf{c}_4 = \begin{pmatrix} 0 \\ -1 \end{pmatrix}, \qquad \mathbf{c}_5 = \begin{pmatrix} 0 \\ 0 \end{pmatrix}.$$

In each of these channels, we consider an exclusion principle, i.e. we allow at most one cell per channel. We denote by $\tilde{b} = b + b_0$ the total number of channels per node which can be occupied simultaneously, where b_0 is the number of channels with zero velocity (rest channels), here $b_0 = 4$.[3] In our LGCA, we represent healthy tissue by the empty channels and we

[1] Cadherins: Important class of transmembrane proteins. They play a significant role in cell–cell adhesion, ensuring that cells within tissues are bound together.

[2] Extracellular matrix: Components that are surrounding cells and composed of secreted fibrous proteins (e.g. collagen) and gel-like polysaccharides (e.g. glycosaminoglycans) binding cells and tissues together.

[3] The value of the number of rest channels b_0 is defined upon scaling of the model to a corresponding experiment or *in vivo* situation. Since the model is not representing any specific experiment, the choice of b_0 remains arbitrary here and qualitatively identical results were obtained for tests with different choices.

model explicitly two cell "species", denoted by $\sigma \in \Sigma = \{C, N\}$: tumor cells (C) and necrotic (N) entities, respectively. We allow the movement of these populations in two different parallel [22] lattices $\mathcal{L}_\sigma \sim \mathcal{L}$. We represent the channel occupancy by a Boolean random variable called *occupation number* $\eta_{\sigma,i}(\mathbf{r}, k) \in \{0, 1\}$, where $i = 1, \ldots, \tilde{b}, \sigma \in \Sigma$ for tumor cells and necrotic entities, $\mathbf{r} \in \mathbb{Z}^2$ the spatial variable and $k \in \mathbb{N}_0$ the time variable. The $\tilde{b}$-dimensional vector

$$\boldsymbol{\eta}_\sigma(\mathbf{r}, k) := (\eta_{\sigma,1}(\mathbf{r}, k), \ldots, \eta_{\sigma,\tilde{b}}(\mathbf{r}, k)) \in \mathcal{E}$$

is called *node configuration* and $\mathcal{E} = \{0, 1\}^{\tilde{b}}$ the automaton *state space*. *Node density* is the total number of cells present at a node $\mathbf{r}$ for a given species σ, and is denoted by

$$n_\sigma(\mathbf{r}, k) := \sum_{i=1}^{\tilde{b}} \eta_{\sigma,i}(\mathbf{r}, k).$$

We can also define a *total node density*, the sum of node densities over all species σ

$$n(\mathbf{r}, k) := \sum_{\sigma=C,N} \sum_{i=1}^{\tilde{b}} \eta_{\sigma,i}(\mathbf{r}, k).$$

The *global configuration* for the lattice of species σ is given by

$$\boldsymbol{\eta}_\sigma(k) := \{\boldsymbol{\eta}_\sigma(\mathbf{r}, k)\}_{\mathbf{r}\in\mathcal{L}}.$$

Finally, the global configuration is $\boldsymbol{\eta}(k) := \{\boldsymbol{\eta}_\sigma(\mathbf{r}, k)\}_{\mathbf{r}\in\mathcal{L},\sigma\in\Sigma}$ and the overall state space is $\{0, 1\}^{\tilde{b}|\Sigma|}$.

2.2. LGCA dynamics

Automaton dynamics arises from the repetition of three rules (operators): propagation (P), reorientation (O) and cell reactions (R). The composition of the three operators R ∘ O ∘ P is applied independently at every node of the lattice at each time step resulting in the next configuration:

$$\eta^{\mathrm{R}\circ\mathrm{O}\circ\mathrm{P}}_{\sigma,i}(\mathbf{r} + m_\sigma \mathbf{c}_i, k + 1) = \mathcal{R}(\eta_{\sigma,i}(\mathbf{r}, k)).$$

In particular, the reorientation and the propagation operators are related to cell motion, while the cell reactions operator controls the change of the local number of cells on a node. In the following, we present these LGCA operators in detail.

2.2.1. Propagation (P)

The process of free streaming of cells of species σ in the medium is modeled by the propagation step. The propagation step is deterministic and is governed by an operator P. By the application of P, all cells are transported simultaneously to nodes in the direction of their velocity, i.e. a cell residing in channel $(\mathbf{r}, \mathbf{c}_i)$ at time k is moved to a neighboring channel $(\mathbf{r} + m_\sigma \mathbf{c}_i, \mathbf{c}_i)$ during one time step. Here $m_\sigma \in \mathbb{N}$ determines the speed and $m_\sigma\ \mathbf{c}_i$ is the translocation of the cell. In our model $m_C = 1$ and $m_N = 0$, since the necrotic cells are considered immobile. The cells residing on the rest channel do not move as they have zero velocity. In terms of occupation numbers, the state of a channel $(\mathbf{r} + m_\sigma \mathbf{c}_i, \mathbf{c}_i)$ after propagation becomes:

$$\eta^{\mathrm{P}}_{\sigma,i}(\mathbf{r} + m_\sigma \mathbf{c}_i, k + 1) = \eta_{\sigma,i}(\mathbf{r}, k).$$

We note that this operator is mass and momentum conserving.

2.2.2. Reorientation (O)

The reorientation operator is responsible for the redistribution of cells within the velocity channels of a node, providing a new node velocity distribution. In this paper, we assume that individual cells perform random walks. The transition probabilities are

$$\mathbb{P}(\boldsymbol{\eta}_\sigma \to \boldsymbol{\eta}^{\mathrm{O}}_\sigma)(\mathbf{r}, k) = \frac{1}{Z}\delta(n_\sigma(\mathbf{r}, k), n^{\mathrm{O}}_\sigma(\mathbf{r}, k)), \tag{1}$$

where the normalization factor $Z = \sum_{\boldsymbol{\eta}^{\mathrm{O}}(r,k)} \delta\big(n(\mathbf{r}, k), n^{\mathrm{O}}(\mathbf{r}, k)\big)$ corresponds to the equivalence class defined by the value of the pre-interaction node density $n(\mathbf{r}, k)$. Obviously, this case implies a random redistribution of the cells among the node's channels. The Kronecker δ assumes the mass conservation of this operator. Our choice for the reorientation operator is one out of various possible ways to describe random motion by means of LGCA [16,21]. The particular choice of the rule greatly simplifies the subsequent analytical derivation of the equations describing the macro- and mesoscopic evolution of the automaton.

2.2.3. Cell reactions (R)

In this section, we define the interactions between the two cell species and the interactions among individuals of each species. Generally, the definition of these interactions is a difficult and ambitious task. For *in vivo* tumors the complexity of the interaction phenomena cannot be captured easily by computational models. In our model, we try to include the most important features of tumor growth and we attempt to approximate the cell interactions. In this study, an important modeling assumption is that we relate the free space to nutrient availability.

- **Tumor cells**: Here, two processes are taken into account: *mitosis* and *necrosis*.
  - *Mitosis* is the cell-doubling process. We assume that tumor cells can divide only if they have just a few competitors on the node (less competition for nutrients), i.e. the node density of tumor cells $n_C(\mathbf{r}, k)$ should be lower than a threshold $\theta_M \in (0, \tilde{b})$. The fixed probability of mitosis r_M could potentially be a function of tumor node density.
  - *Necrosis* is the decay of tumor cells due to nutrient depletion. Analogous to the above, if the total node density exceeds $\theta_N \in [1, \tilde{b})$, then we assume that the nutrient consumption is critical and leads to tumor cell necrosis. The fixed necrosis probability r_N could be a function of $n_C(\mathbf{r}, k)$ and can be defined in various ways following *in vivo* and *in vitro* observations.

  Now, we define the new node density after the action of the reaction operators for the tumor cells:

$$n_C^{\mathrm{R}}(r, k) := \begin{cases} n_C(\mathbf{r}, k) + 1, & \text{w. p. } r_M \text{ if } n_C(\mathbf{r}, k) \le \theta_M \\ n_C(\mathbf{r}, k) - 1, & \text{w. p. } r_N \text{ if } n_C(\mathbf{r}, k) \ge \theta_N \\ n_C(\mathbf{r}, k), & \text{else,} \end{cases} \tag{2}$$

  where w. p. denotes "with probability". It is easy to observe that tumor cells undergo a birth–death process with corresponding probabilities $r_M, r_N \in (0, 1) \subset \mathbb{R}$.
- **Necrotic entities**: Necrotic entities are produced from tumor cells by the process of necrosis, i.e. due to nutrient depletion within a node. The new node density of the necrotic entities is given by

$$n_N^{\mathrm{R}}(\mathbf{r}, k) := \begin{cases} n_N(\mathbf{r}, k) + 1, & \text{w. p. } r_N \text{ if } n_C(\mathbf{r}, k) \ge \theta_N \wedge n_N(\mathbf{r}, k) < \tilde{b}, \\ n_N(\mathbf{r}, k), & \text{else.} \end{cases} \tag{3}$$

  Hence necrotic entities undergo a birth process with probability r_N. Obviously, necrotic entities play a passive role in the evolution of the tumor. Finally, we note that once created, necrotic entities do not move. Note that it is reasonable to assume that $\theta_M < \theta_N$.

2.3. Micro-dynamical equations

Following the above description of the automaton rules, we next derive the micro-dynamical description of our LGCA. The post-reaction state $\eta_{\sigma,i}^{\mathrm{R}}(\mathbf{r}, k)$ after the application of the reaction operator is:

$$\eta_{\sigma,i}^{\mathrm{R}}(\mathbf{r}, k) = \mathcal{R}_{\sigma,i}(\eta_{C,i}(\mathbf{r}, k), \eta_{N,i}(\mathbf{r}, k)), \tag{4}$$

where $\mathcal{R}_{\sigma,i} : \mathcal{E} \to \mathcal{E}$. In particular, Eq. (4) can be written as:

$$\eta_{C,i}^{\mathrm{R}} = \eta_{C,i} + \xi_{C,i}\tilde{\eta}_{C,i}\Theta(\theta_M - n_C) - \xi_{N,i}\eta_{C,i}\Theta(n_C - 1 - \theta_N) \tag{5}$$

$$\eta_{N,i}^{\mathrm{R}} = \eta_{N,i} + \xi_{N,i}\tilde{\eta}_{N,i}\Theta(n_C - \theta_N), \tag{6}$$

where we have dropped the space and time dependence for simplicity and used the notation $\tilde{\eta}_{\sigma,i} = 1 - \eta_{\sigma,i}$. The $\xi_{\sigma,i}$ are random Boolean variables which represent the realization of a mitotic or a necrotic event, with $\sum_{i=1}^{\tilde{b}} \xi_{\sigma,i} = 1$, and the corresponding probabilities are $\mathbb{P}(\xi_{C,i} = 1) = r_M/\tilde{b}$ and $\mathbb{P}(\xi_{N,i} = 1) = r_N/\tilde{b}$. The Heaviside function $\Theta(\cdot)$ is defined as:

$$\Theta(x) = \begin{cases} 1, & \text{if } x \ge 0 \\ 0, & \text{else.} \end{cases}$$

The complete spatio-temporal automaton dynamics are described by the following **micro-dynamical difference equations**:

$$\eta_{\sigma,i}(\mathbf{r} + m_\sigma \boldsymbol{c_i}, k + 1) - \eta_{\sigma,i}(\mathbf{r}, k) = \eta_{\sigma,i}^{\mathrm{RoO}}(\mathbf{r}, k) - \eta_{\sigma,i}(\mathbf{r}, k) = C_{\sigma,i}(\boldsymbol{\eta}_\sigma(\mathbf{r}, k)) \tag{7}$$

for $m_\sigma \in \mathbb{N}, \sigma \in \Sigma$ and $i = 1, \ldots, \tilde{b}$. The term $C_{\sigma,i}(\boldsymbol{\eta}_\sigma(\mathbf{r}, k))$ is called **collision operator** and takes the values $\{-1, 0, 1\}$. Details of the collision operator can be found in the Appendix.

3. Results

In this section, we focus on the numerical and the mathematical analysis of our tumor model. Firstly, we present simulation results with special emphasis on the system's pattern formation potential. Subsequently, by means of a cut-off mean-field analysis, we derive a macroscopic description of our LGCA. Finally, we analytically calculate the speed of the invasive front.

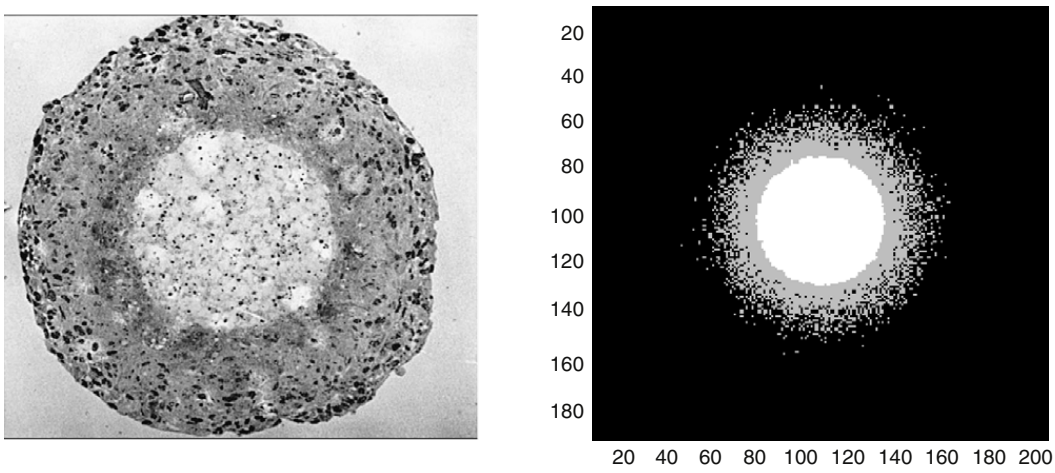

Fig. 1. Left: Typical spatio-temporal pattern formation of *in vitro* tumors (reprinted with permission from Folkmann et al. [23]). One observes clearly the presence of a necrotic core and an outer rim of proliferative tumor cells. **Right**: A LGCA simulation exhibits a similar structure. In the simulation, tumor cells are depicted in grey, necrotic entities in white, and empty nodes in black.

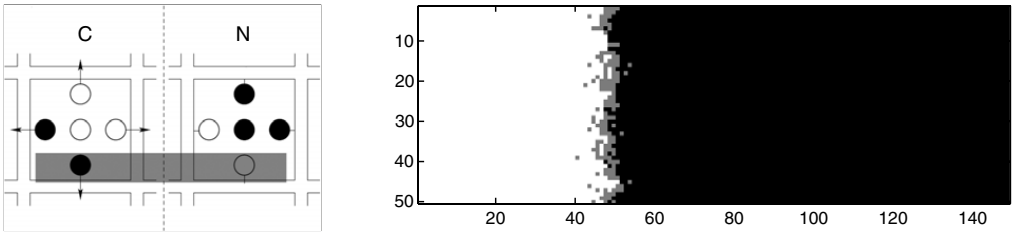

Fig. 2. Left: Two corresponding nodes at position **r**, one from the tumor and the other from the necrotic lattice. The grey stripe denotes one chosen pair of channels. **Right**: Spatio-temporal pattern formation in the LGCA model. An invading two-dimensional tumor wavefront for $r_M = 0.2$ and $r_N = 0.7$. Tumor cells are depicted in grey, necrotic entities in white, and empty nodes in black.

3.1. Simulations

In Fig. 1, we observe the typical pattern formation of our system: the expansion of the tumor front precedes the necrotic core because necrotic entities are created when the tumor cell density reaches the critical threshold θ_N. This pattern coincides with medical *in vivo* and *in vitro* observations, where typically, tumors form a thin proliferating rim followed by a necrotic core [23].

For further analysis a simplified, effectively one-dimensional geometry is introduced. We employ two identical square lattices $\mathcal{L}_\sigma = L_1 \times L_2$ (L_1 represents the horizontal and L_2 the vertical axis of the lattice $\mathcal{L}_\sigma$, respectively), for each cell species. The system is open at the right boundary of the L_1-axis and we impose zero-flux boundary conditions at the left boundary of the lattices. In the L_2-axis periodic boundary conditions are set. The initial condition (I.C.) is a fully occupied stripe of tumor cells at the beginning of the L_1-axis. The result of our simulations is a propagating two-dimensional front along the L_1-axis, mimicking "growth inside a tube" (Fig. 2). The quasi-one-dimensional setting has the following advantages:

- In order to study the traveling front, we reduce our two-dimensional system to one dimension, by averaging the concentration profile of each species along the L_2-axis, i.e. $n_x(k) = n(r_x, k) = \frac{1}{|L_2|} \sum_{r_y \in |L_2|} n(\mathbf{r}, k)$. Fig. 3 (left) shows that this simple model is able to create a traveling front that invades into the empty lattice nodes (healthy tissue).
- The front is well defined as the mean position of the foremost cells.
- The front profile relaxes to an almost steady-state shape, which moves almost uniformly along the L_1-axis.

Finally, we observe that the tumor front evolves linearly in time, as shown in the right panel of Fig. 3.

3.2. Mean-field analysis

In this section, we analyze the behavior of our tumor LGCA model. We derive a partial differential equation that corresponds to the automaton's macroscopic behavior, by means of a mean-field approximation. Subsequently, we introduce a cut-off in the mean-field description and we calculate the speed of the invasive front.

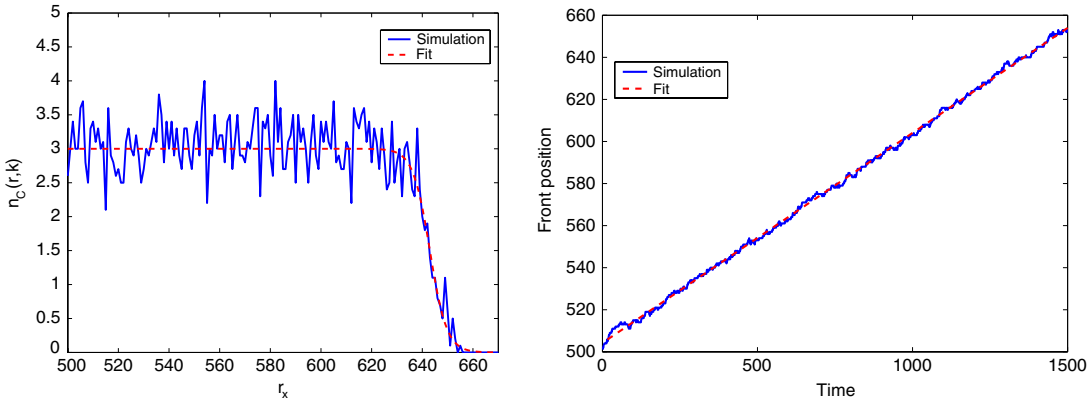

Fig. 3. **Left**: Snapshot of the average concentration profile along the L_1-axis, i.e. $n_x(k) = n(r_x, k) = \frac{1}{|L_2|}\sum_{r_y \in |L_2|} n(\mathbf{r}, k)$. **Right**: Front position denotes the distance of the front from its initial position. The slope of the line defines the speed of the tumor invasion. Here, we observe the tumor "grows" linearly, i.e. the tumor front invades the host with a constant speed.

3.2.1. *The nonlinear Lattice Boltzmann equation*

Let us define the **single particle distribution functions**, which are the average values of the $\eta_{\sigma,i}$, i.e. the average channel occupation number, by

$$f_{\sigma,i}(\mathbf{r}, k) = \langle \eta_{\sigma,i}(\mathbf{r}, k)\rangle = \sum_{\boldsymbol{\eta}_\sigma} \eta_{\sigma,i}(\mathbf{r}, k)\mathbb{P}_k(\boldsymbol{\eta}_\sigma(\mathbf{r})),$$

where $f_{\sigma,i}(\mathbf{r}, k) \in [0, 1]$, $i = 1, \ldots, \tilde{b}$. Note that the average $\langle \ldots \rangle$ is defined over an arbitrary node distribution $\mathbb{P}_k(\boldsymbol{\eta}_\sigma(\mathbf{r}))$ at time k.

Moreover, we define the *mean node density* as

$$\rho_\sigma(\mathbf{r}, k) = \langle n_\sigma(\mathbf{r}, k)\rangle = \sum_{i=1}^{\tilde{b}} f_{\sigma,i}(\mathbf{r}, k).$$

Applying the mean-field or Boltzmann approximation (Stoßzahlansatz), we can write down the **completely factorized** $\mathbb{P}_k$ distribution

$$\mathbb{P}_k(\boldsymbol{\eta}_\sigma(\mathbf{r})) = \prod_{i=1}^{\tilde{b}} \mathbb{P}_k(\eta_{\sigma,i}(\mathbf{r})) = \prod_{i=1}^{\tilde{b}} f_{\sigma,i}(\mathbf{r})^{\eta_{\sigma,i}(\mathbf{r})}(1 - f_{\sigma,i}(\mathbf{r}))^{1-\eta_{\sigma,i}(\mathbf{r})}. \tag{8}$$

The mean-field assumption discards all pair or higher on and off node correlations. One can derive from the micro-dynamical description (7) the mean-field approximation for our LGCA, called the **nonlinear Lattice Boltzmann Equation** (LBE)

$$f_{\sigma,i}(\mathbf{r} + m_\sigma \mathbf{c}_i, k + 1) - f_{\sigma,i}(\mathbf{r}, k) = \langle C_{\sigma,i}(\boldsymbol{\eta}(\mathbf{r}, k))\rangle_{MF} = \tilde{C}_{\sigma,i}(\mathbf{f}(\mathbf{r}, k)), \tag{9}$$

where $\mathbf{f}(\mathbf{r}, k) = (\mathbf{f}_C, \mathbf{f}_N) = (f_{C,1}(\mathbf{r}, k), \ldots, f_{C,\tilde{b}}(\mathbf{r}, k), f_{N,1}(r, k), \ldots, f_{N,\tilde{b}}(\mathbf{r}, k))$ and $\tilde{C}_{\sigma,i} \in [-1, 1]$ is called the **expected collision operator**. Given that $m_C = 1$ and $m_N = 0$, since the necrotic entities do not move, we can write the LBE for our model

$$\begin{aligned} f_{C,i}(\mathbf{r} + \mathbf{c}_i, k + 1) - f_{C,i}(\mathbf{r}, k) &= \frac{1}{\tilde{b}}\sum_{j=1}^{\tilde{b}} \langle \eta^{\mathrm{R}}_{C,j}(\mathbf{r}, k)\rangle - f_{C,i}(\mathbf{r}, k) \\ &= \frac{1}{\tilde{b}} F_C(\mathbf{f}_C, \mathbf{f}_N) \end{aligned} \tag{10}$$

$$\begin{aligned} f_{N,i}(\mathbf{r}, k + 1) - f_{N,i}(\mathbf{r}, k) &= \frac{1}{\tilde{b}}\sum_{j=1}^{\tilde{b}} \langle \eta^{\mathrm{R}}_{N,j}(\mathbf{r}, k)\rangle - f_{N,i}(\mathbf{r}, k) \\ &= \frac{1}{\tilde{b}} F_N(\mathbf{f}_C, \mathbf{f}_N). \end{aligned} \tag{11}$$

The F_σ terms can be easily calculated by applying the mean-field approximation to Eqs. (5) and (6).

The steady states with homogeneous occupation, i.e. $f_{\sigma,i} = \bar{f}_\sigma$ can be determined numerically by solving the above expected collision operators when equal to zero (for details see the Eqs. (43) and (44) in the Appendix), i.e.:

$$\tilde{C}_{\sigma,i}(\bar{f}_C, \bar{f}_N) = 0 \Rightarrow (\bar{f}_C, \bar{f}_N) = (0, \alpha) \quad \text{or } (g(r_M, r_N), 1), \tag{12}$$

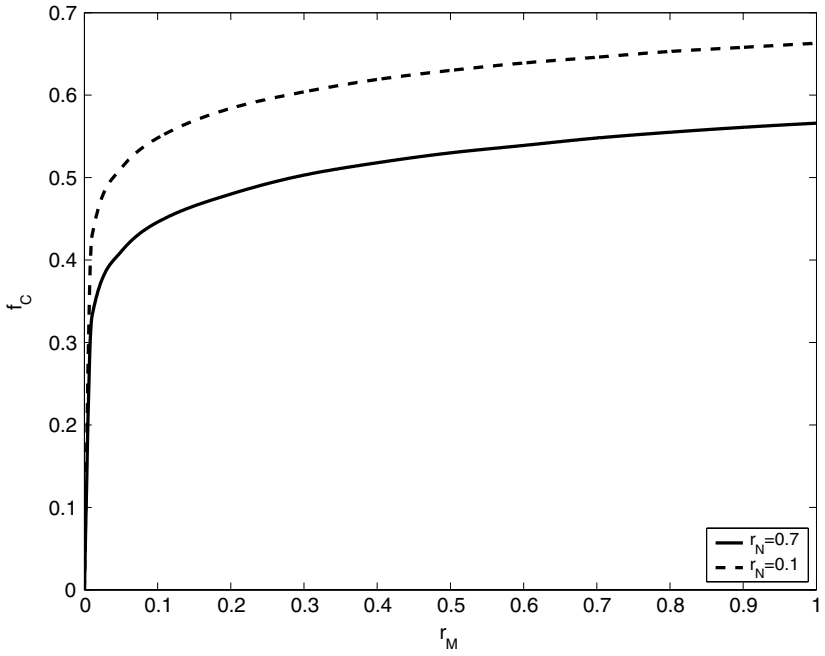

Fig. 4. The second steady-state solution of the tumor cells $\bar{f}_C = g(r_M, r_N)$ for different values of mitotic and necrotic probabilities. The mitotic and the necrotic thresholds are $\theta_M = 4$ and $\theta_N = 6$, respectively.

where $\alpha \in [0, 1]$ is a free parameter and g a real function numerically determined, depending on the parameters r_M and r_N (Fig. 4). The first fixed point represents the tumor-free situation. The second fixed point $(g, 1)$ corresponds to a well-defined necrotic core. The maximum number of tumor cells allowed to survive on a node that belongs to the necrotic core is equal to g.

For a given average number of cells per node $\bar{\rho}_\sigma$ the nonlinear LBE has a stationary and isotropic solution $\bar{f}_\sigma = \frac{\bar{\rho}_\sigma}{\tilde{b}} = \bar{u}_\sigma$. By eliminating the spatial effect, i.e by setting $m_\sigma = 0$, Eq. (10), (11) can be considered as a discretization of the ODEs

$$\frac{\mathrm{d}u_C}{\mathrm{d}t} = \frac{1}{\tilde{b}} F_C(u_C, u_N) \tag{13}$$

$$\frac{\mathrm{d}u_N}{\mathrm{d}t} = \frac{1}{\tilde{b}} F_N(u_C, u_N), \tag{14}$$

where F_C, F_N are the rates of change of tumor cells and necrotic entities, respectively, expressed in terms of density per channel. The homogeneous, isotropic solutions $(\bar{f}_C, \bar{f}_N)$ of the LBE coincide with the fixed points of Eq. (13), (14).

3.2.2. Solutions of the linearized LBE

In order to gain insight into the behavior of the nonlinear LBE, we study small deviations from a steady state by linearizing around the homogeneous steady-state solution. We define the **single particle distribution fluctuations** by

$$\delta f_{\sigma,i}(\mathbf{r}, k) = f_{\sigma,i}(\mathbf{r}, k) - \bar{f}_\sigma. \tag{15}$$

We linearize the nonlinear LBE around a steady state $(\bar{f}_C, \bar{f}_N)$ and construct the matrix $\mathbf{\Omega}^0$ with elements

$$\mathbf{\Omega}^0_{ij} = \left. \frac{\partial \tilde{C}_{\sigma,i}(\mathbf{r}, k)}{\partial \delta f_{\sigma,j}(\mathbf{r}, k)} \right|_{\bar{f}_\sigma}, \quad i, j = 1, \ldots, \tilde{b}. \tag{16}$$

The matrix Ω^0 takes the form

$$\mathbf{\Omega}^0 = \begin{pmatrix} \dfrac{\partial \tilde{C}_{C,i}}{\partial \delta f_C} & | & \dfrac{\partial \tilde{C}_{C,i}}{\partial \delta f_N} \\ -- & | & -- \\ \dfrac{\partial \tilde{C}_{N,i}}{\partial \delta f_C} & | & \dfrac{\partial \tilde{C}_{N,i}}{\partial \delta f_N} \end{pmatrix}_{(f_C, f_N) = (\bar{f}_C, \bar{f}_N)}$$

with dimension $|\Sigma|\tilde{b} \times |\Sigma|\tilde{b}$ and the four block matrices have dimension $\tilde{b} \times \tilde{b}$, with $|\Sigma| = 2$ and $\tilde{b} = 8$. Hence, the linearized LBE is:

$$\delta f_{\sigma,i}(\mathbf{r} + m_\sigma \mathbf{c}_i, k+1) - \delta f_{\sigma,i}(\mathbf{r}, k) = \sum_{j=1}^{\tilde{b}} \mathbf{\Omega}^0_{ij} \delta f_{C,j}(\mathbf{r}, k) + \sum_{j=\tilde{b}+1}^{2\tilde{b}} \mathbf{\Omega}^0_{ij} \delta f_{N,j-\tilde{b}}(\mathbf{r}, k). \tag{17}$$

Rearranging the terms of Eq. (17) we obtain:

$$\delta f_{\sigma,i}(\mathbf{r} + m_\sigma \mathbf{c}_i, k+1) = \sum_{j=1}^{\tilde{b}} \mathbf{\Gamma}_{ij}(\mathbf{r}, k) \delta f_{C,j}(\mathbf{r}, k) + \sum_{j=\tilde{b}+1}^{2\tilde{b}} \mathbf{\Gamma}_{ij}(\mathbf{r}, k) \delta f_{N,j-\tilde{b}}(\mathbf{r}, k), \tag{18}$$

with

$$\mathbf{\Gamma}_{ij} = \delta_{ij} + \mathbf{\Omega}^0_{ij}, \tag{19}$$

where the matrix $\mathbf{\Gamma} = (\mathbf{I} + \mathbf{\Omega}^0)$ is called the **Boltzmann propagator** which describes how small deviations from the $\bar{f}_\sigma$ evolve when the interaction operator R is applied on a node.

We choose as a linearization point the steady state (0,0), which represents the healthy tissue into which the tumor invades. Note that the behavior of the tumor at the tip of the invasive front is not influenced by the presence of the necrotic core, since this is developed far from the invasive zone, as shown in simulations. Moreover, the established necrotic region is related to the second steady state $(g, 1)$, where $g > 0$ (see Fig. 4). The invasion point is defined as the boundary between tumor cells and healthy tissue, corresponding the steady state (0,0).

After the linearization, the entries of the diagonal block matrices of the matrix $\mathbf{\Omega}^0$ are non-zero and all the others equal zero. The propagator $\mathbf{\Gamma}$ takes the form

$$\mathbf{\Gamma} = \mathbf{I} + \mathbf{\Omega}^0 = \begin{pmatrix} \omega_1 & | & 0 \\ -- & | & -- \\ 0 & | & \omega_4 \end{pmatrix},$$

where $\omega_1, \omega_4 \in \mathbb{R}_+$ are parameters to be defined below. The Boltzmann equation reads:

$$\delta f_{C,i}(\mathbf{r} + m_C \mathbf{c}_i, k+1) = \omega_1 \sum_{j=1}^{\tilde{b}} \delta f_{C,j}(\mathbf{r}, k) \tag{20}$$

$$\delta f_{N,i}(\mathbf{r} + m_N \mathbf{c}_i, k+1) = \omega_4 \sum_{j=1}^{\tilde{b}} \delta f_{N,j}(\mathbf{r}, k), \tag{21}$$

where $i = 1, \ldots, \tilde{b}$. Now, we insert the Fourier transform with wavenumber $\mathbf{q} = (q_1, q_2)$ of the corresponding Fourier mode:

$$\delta f_{\sigma,i}(\mathbf{r}, k) = A^k \mathrm{e}^{\mathrm{i}\langle \mathbf{q}, \mathbf{c}_i \rangle m_\sigma} \delta f_{\sigma,i}, \tag{22}$$

where $\langle \cdot, \cdot \rangle$ is the inner product of two vectors. Then we obtain the following algebraic set of equations for the $\delta f_{\sigma,i}$'s:

$$\sum_{j=1}^{2\tilde{b}} \mathbf{M}_{ij} \delta f_{\sigma,i} = 0, \quad i = 1, \ldots, \tilde{b}, \tag{23}$$

where the $\mathbf{M}$ matrix is a block diagonal matrix with block matrices of 8×8 dimension, and its form is:

$$\mathbf{M} = \begin{pmatrix} -A\mathrm{e}^{\mathrm{i}\langle \mathbf{q}, \mathbf{c}_i \rangle m_\sigma} \delta_{ij} + \omega_1 & | & 0 \\ - - - - - - - - & | & - - - - - - - - \\ 0 & | & -A\delta_{ij} + \omega_4 \end{pmatrix},$$

A non-trivial solution exists if $\det(\mathbf{M}) = 0$. Making explicit use of this condition, we obtain a 16th order polynomial equation for the damping coefficient A:

$$A^{16} - 2A^{15}(\omega_1 \cos(q_1) + \omega_1 \cos(q_2) + 4\omega_4 + 2\omega_1) + 16A^{14}\omega_1\omega_4(\cos(q_1) + \cos(q_2) + 2) = 0. \tag{24}$$

The solutions of A for the above discrete dispersion relation are:

$A^{(1)}(\mathbf{q}) = 2\omega_1 \cos(q_1) + 2\omega_1 \cos(q_2) + 4\omega_1,$
$A^{(2)}(\mathbf{q}) = 8\omega_4,$
$A^{(j)}(\mathbf{q}) = 0, \quad \text{for } j = 3, \ldots, 16.$

The damping coefficients $A^{(1)}$ and $A^{(2)}$ depend on $\mathbf{q}$ and their value is different from zero. Then

$$\sum_{j=1}^{\tilde{b}} \mathbf{\Gamma}_{ij} = \sum_{j=1}^{\tilde{b}} (\delta_{ij} + \mathbf{\Omega}^0_{ij}) = \tilde{b}\omega_l \Leftrightarrow \omega_l = \frac{1}{\tilde{b}} \left(1 + \sum_{j=1}^{\tilde{b}} \mathbf{\Omega}^0_{ij} \right) \tag{25}$$

for $l = 1, 4$ and $i = 1, \ldots, \tilde{b}$. Following Boon et al. [24] one realizes that

$$\sum_{j=1}^{\tilde{b}} \mathbf{\Omega}^0_{ij} = \frac{1}{\tilde{b}} \frac{\mathrm{d}F_\sigma(\bar{\mathbf{u}})}{\mathrm{d}\bar{\mathbf{u}}} = -\kappa_\sigma, \tag{26}$$

i.e. κ_σ is the linearized phenomenological rate around the fixed-point solution $\bar{\boldsymbol{u}} = (\bar{u}_C, \bar{u}_N)$. Around the equilibrium point (0,0), we have $\kappa_C = -r_M$, $\kappa_N = 0$. Therefore:

$$\omega_1 = \frac{1}{\tilde{b}}(1 + r_M),$$
$$\omega_4 = \frac{1}{\tilde{b}}.$$

The damping coefficient $A^{(2)} = 1$ indicates a neutral stability against perturbations in the necrotic population, since necrotic entities, in the absence of tumor cells, do not proliferate, decay or migrate. Hence, the front propagation is solely driven by the linear instability $A^{(1)} > 1$ of the empty lattice against a perturbation with tumor cells.

For small wavenumbers $|\mathbf{q}| \to 0$ and for infrequent cell divisions ($r_M \ll 1$) the damping coefficient $A^{(1)}$ can be expressed as the exponential of an equivalent continuous damping rate $z(\mathbf{q})$, i.e. $A^{(1)}(\mathbf{q}) = \mathrm{e}^{z(\mathbf{q})}$ or

$$z(\mathbf{q}) = \ln(A^{(1)}(\mathbf{q})) = \ln(1 + r_M) - \frac{1}{\tilde{b}}|\mathbf{q}|^2 + O(|\mathbf{q}|^4). \tag{27}$$

For small mitotic rates $r_M \ll 1$, the diffusion is sufficiently rapid compared to reactions. Therefore, we can consider that reactions act as a perturbation of the diffusion process. Thus, for small mitotic rates the discrete rate law will closely approximate the continuous phenomenological rate [25]. The above equation shows that in this regime the dispersion relation is equivalent to that of the linearized reaction–diffusion equation:

$$\frac{\partial \delta u_C}{\partial t}(\mathbf{x}, t) = D\nabla^2 \delta u_C(\mathbf{x}, t) + \frac{1}{\tilde{b}} \frac{\mathrm{d}F_\sigma(\bar{\mathbf{u}})}{\mathrm{d}\bar{\mathbf{u}}} \delta u_C(\mathbf{x}, t) \tag{28}$$

with $D = 1/\tilde{b} = 1/8$ and $(\mathbf{x}, t) \in \mathbb{R}^2 \times \mathbb{R}^+$ the continuous spatio-temporal variables. In this equation the field $\delta u_C(\mathbf{x}, t) = u_C(\mathbf{x}, t) - \bar{u}_C$ is the mass density fluctuation per channel on the lattice.

The continuous linearized reaction–diffusion equation (28) describes the time evolution of small perturbations around the fixed point $\bar{u}_C = 0$. Thus the fluctuations are $\delta u_C(\mathbf{x}, t) = u_C(\mathbf{x}, t)$, the linearized rate $\frac{1}{\tilde{b}} \frac{\mathrm{d}F_\sigma(\bar{\mathbf{u}})}{\mathrm{d}\bar{\mathbf{u}}} = -\kappa_C = r_M$ and the Eq. (28) multiplied by $\tilde{b}$ can be rewritten as:

$$\frac{\partial \rho_C}{\partial t}(\mathbf{x}, t) = D\nabla^2 \rho_C(\mathbf{x}, t) + r_M \rho_C(\mathbf{x}, t). \tag{29}$$

The above equation provides a macroscopic description of the tumor's spatio-temporal evolution around the fixed point $\rho_C = 0$ for small mitotic rates. When no tumor cells are present, the necrotic population remains unchanged, i.e. $\frac{\partial \rho_N}{\partial t}(\mathbf{x}, t) = 0$.

3.2.3. Cut-off mean-field approximation

The spatio-temporal mean-field approximation (29) agrees qualitatively with the system's linearized macroscopic dynamics. However, it fails to provide satisfactory quantitative predictions since it neglects the correlations built by the local fluctuating dynamics. Studies on chemical fronts have shown that these fluctuations may significantly affect the propagation velocity of the wavefront [26,27].

In order to improve the mean-field approximation (here we characterize it as "naive"), we introduce the *cut-off mean-field approach* [28,29]. The idea is that the mean-field continuous equation (29) fails to describe the behavior of individual cells due to their strong fluctuations at the tip of the front [26]. Therefore, we derive the cut-off continuous approach which describes the system up to a threshold density δ of the order of magnitude of one cell, i.e. $\delta \sim \mathcal{O}(1/\tilde{b})$. First assume that the full nonlinear reactive dynamics can be described by a term $F_C(\rho_C, \rho_N)$. Then, the fully nonlinear cut-off MF equation reads

$$\partial_t \rho_C = D\nabla^2 \rho_C + F_C(\rho_C, \rho_N)\Theta(\rho - \delta), \tag{30}$$

where $\Theta(\cdot)$ is a Heaviside function. Clearly, if we set $\delta = 0$ then the cut-off PDE will coincide with the naive mean-field approximation.

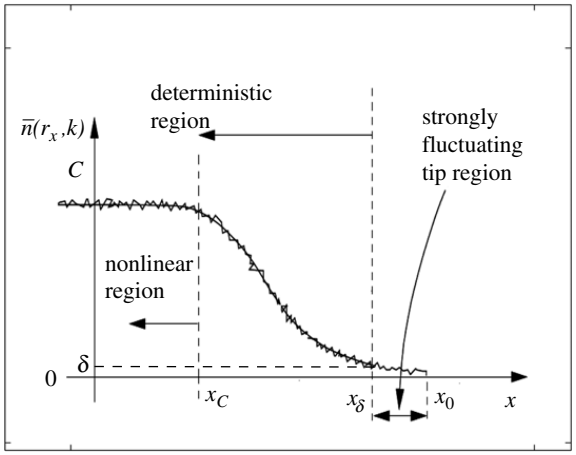

Fig. 5. A sketch of the wavefront as shown in Fig. 3 (left). We distinguish three regimes: (i) $x \in [x_\delta, x_0]$, where $0 < \rho(x) < \delta$: the region represents a highly fluctuating zone, where the cells perform a random walk with almost no proliferation, (ii) $x \in [x_C, x_\delta]$, where $\delta < \rho(x) < C$: this region is a result of nonlinear proliferation and cell diffusion and (iii) $x \in [0, x_C]$, where $\rho(x) \simeq C$: this regime represents the bulk of the front (saturated lattice) where no significant changes are observed.

The cut-off macroscopic description (30) adds an extra fixed point, i.e. $\rho(x_i) = \{0, \delta, C\}, i = 0, \delta, C$ (by C we denote the maximum occupation defined by the function $g(r_M, r_N)$ shown in Fig. 4) which divide the front in the three following regions (Fig. 5):

(i) $x \in [x_\delta, x_0]$, where $0 < \rho_C(x) < \delta$: this regime represents a highly fluctuating zone, where the cells perform a random walk with almost no proliferation.
(ii) $x \in [x_C, x_\delta]$, where $\delta < \rho_C(x) < C$: this region is a result of nonlinear proliferation and cell migration.
(iii) $x \in [0, x_C]$, where $\rho_C(x) \simeq C$: this region represents the bulk of the front (saturated lattice) where no significant changes are observed.

In order to characterize the linearized tumor dynamics at the front, we modify the LBE for the tumor cells:

$$f_{C,i}(\mathbf{r} + \mathbf{c}_i, k+1) - f_{C,i}(\mathbf{r}, k) = \sum_{j=1}^{\tilde{b}} \left(\frac{1}{\tilde{b}} - \delta_{ij} \right) f_{C,j}(\mathbf{r}, k) + \frac{1}{\tilde{b}} \sum_{j=1}^{\tilde{b}} \left[\langle \eta^{\mathrm{R}}_{C,j}(\mathbf{r}, k) \rangle - f_{C,j}(\mathbf{r}, k) \right] \Theta(\rho - \delta), \tag{31}$$

where the first summation of the rhs accounts for the reorientation dynamics and the second term is the reactive term of the LBE. Intuitively, the Θ-function "cuts off" the reaction term for local densities lower than the threshold δ. Therefore, for $\rho_C < \delta$ the cells are influenced only by the random walk dynamics. Moreover from Eq. (31), we can easily deduce the nonlinear reaction term of Eq. (30):

$$F_C(\rho_C, \rho_N) = \sum_{j=1}^{\tilde{b}} \left[\langle \eta^{\mathrm{R}}_{C,j}(\mathbf{r}, k) \rangle - f_{C,j}(\mathbf{r}, k) \right]. \tag{32}$$

3.3. Traveling tumor front analysis

In this subsection our goal is to analyze and characterize analytically the observed traveling front behavior. We consider that our system evolves in a "tube", as in Fig. 2. Moreover, we make the following assumptions:

(A1) the isotropic evolution of the system allows for the dimension reduction of the analysis to one dimension,
(A2) the system evolves for asymptotically long times, and
(A3) the initial front is sufficiently steep.

Under the assumptions (A1)–(A3), we can consider that the front relaxes to a time invariant profile. Thus, assuming the translational invariance of the system along the front propagation axis L_1, we investigate the steady-state front solutions. The main observable is the average density profile along the axis L_1, i.e.

$$\rho_C(x, t) = \frac{1}{|L_2|} \int_0^{|L_2|} \rho_C(x, y, t)\, \mathrm{d}y \in [0, \tilde{b}]. \tag{33}$$

Substituting the traveling front solution into Eq. (29), $\rho_C(x, t) = U_C(x - vt)$, where $x \in L_1$ and v the front velocity, we obtain:

$$DU_C'' + vU_C' + \left. \frac{\mathrm{d}\tilde{F}_C}{\mathrm{d}U_C} \right|_{U_C = 0} = 0, \qquad \lim_{\xi \to -\infty} u_C = U_C^{\max}, \qquad \lim_{\xi \to +\infty} U_C = 0, \quad U_C' < 0, \tag{34}$$

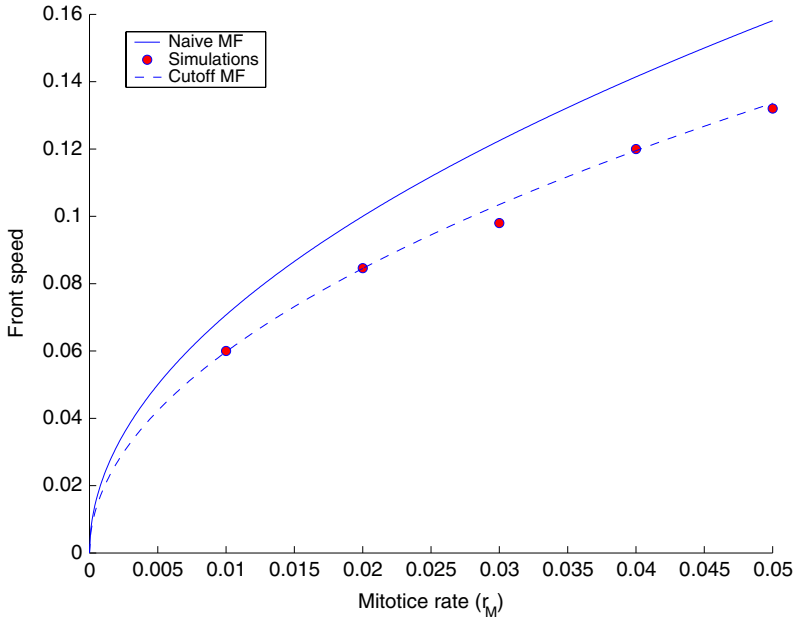

Fig. 6. Comparison of the calculated front speed for the naive and the cut-off MF, i.e. v_n and v_c respectively, against simulations. We observe that the cut-off MF predicts quantitatively the front speed calculated from the simulations for $K \simeq 0.85$.

where the co-moving coordinate $\xi = x - vt$ and the prime denotes the derivative with respect to the variable ξ. The term $\tilde{F}_C$ represents the reaction terms in the naive MF approximation expressed in terms of U_C and U_N. The front speed for the naive MF can be calculated following the classical methodology [30,31], i.e.

$$v_n = 2\sqrt{Dr_M}. \tag{35}$$

The above speed estimation overestimates the actual front speed found in the simulations. In particular, this is the maximum asymptotic value that the discrete front speed can acquire [28] (see also Fig. 6).

The calculation of the front speed for the cut-off MF approximation is more challenging. Following the results proposed by Brunet et al. [28,32], we can obtain an estimate for the cut-off front speed:

$$v_c = 2\sqrt{Dr_M}\left(1 - \frac{K}{\ln^2(\delta)}\right). \tag{36}$$

The cut-off front speed estimation includes a correction factor $1-\frac{K}{\ln^2(\delta)}$, which allows for a better approximation of the actual front speed calculated from the LGCA simulations. The above equation provides a satisfactory description of the system up to the resolution of δ, i.e. to the order of one cell. A reasonable choice of the cut-off would be $\delta = 1/\tilde{b}$. The parameter K is fitted to match quantitatively the simulation results. Several studies have attempted to find an analytical estimate of K but till now this remains an open problem [32]. The cut-off mean-field approximation is a heuristic-phenomenological approach which mimics the leading-order effect of finite population fluctuations by introducing a cut-off in the MF equation. In Fig. 6, we show a comparison of the front speed for varying proliferation rates r_M calculated by the naive MF and the cut-off MF against the front speed obtained from simulations. We observe that for an appropriate choice of K the cut-off MF predicts quantitatively the simulated front speed for all parameter values and a fixed choice of K.

Another important aspect of the invasive behavior is the width of the front. From Fig. 5, we observe that there exists on the front an inflection point $x = x^*$ where the derivatives $\partial_x^{(2n)}\rho_C|_{x=x^*} = 0$ and $n \in \mathbb{N}$. Typically, this inflection point is found at the middle of the front profile, i.e. $\rho_C(x^*) = \tilde{b}g/2$, where $g = \tilde{f}_C$ refers to the bulk fixed point given in Eq. (12) and g can be identified from Fig. 4. The one-dimensional, nonlinear cut-off MF approximation of the LGCA (30) at point $x = x^*$ reads:

$$\partial_t \rho_C|_{x=x^*} = [F(\rho_C, \rho_N)\Theta(\rho - \delta)]|_{x=x^*}. \tag{37}$$

We transform coordinates into $\xi = x - vt$. Then Eq. (37) is evaluated at the point $\xi^* = x^* - vt$ yielding:

$$-vU_C'|_{\xi=\xi^*} = \tilde{F}(U_C, U_N)|_{\xi=\xi^*}, \tag{38}$$

where the Heaviside function is equal to one, since $U_C(\xi^*) > \delta$. The width of the front is:

$$W = -\frac{1}{U_C'|_{\xi=\xi^*}} = \frac{v}{\tilde{F}(U_C, U_N)|_{\xi=\xi^*}}. \tag{39}$$

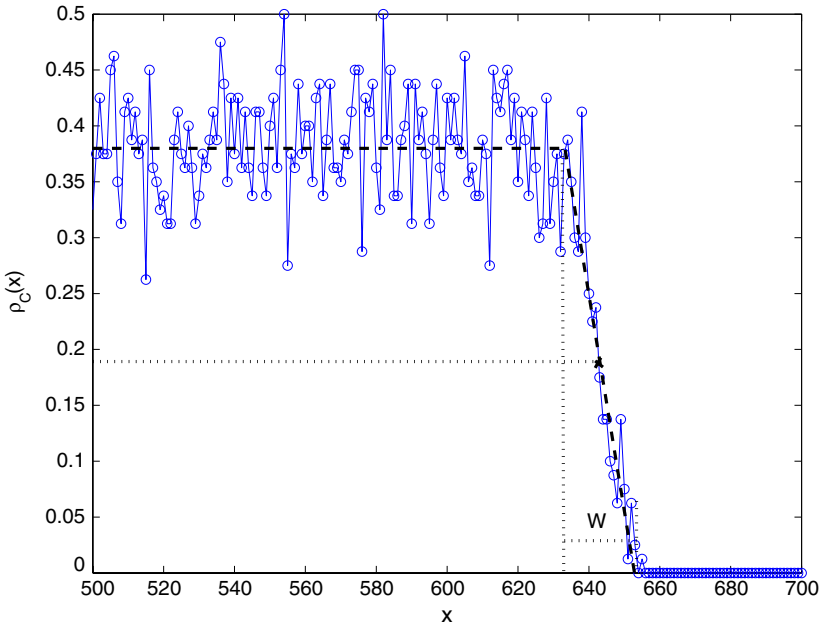

Fig. 7. Numerically the front width is estimated by fitting a straight line, tangential to the inflection point $\rho_C(x^*) = \tilde{b}g/2$ and the front width W is approximated as the inverse slope of the fitted line. In this example, the simulation time is 1500 steps, the mitotic rate $r_M = 0.03$, necrotic rate $r_N = 0.7$, $|L_2| = 10$ and $g \simeq 0.38$ (it can be estimated from Fig. 4). The black, dotted lines are a piecewise linear fit of the front that allows for the estimation of W.

We observe the width of front is proportional to the front speed v. In order to calculate $\tilde{F}(U_C, U_N)|_{\xi=\xi^*}$, we use a uniform channel density $f_{C,i} = \rho_C(x^*)/\tilde{b} = g/2$ for $i = 1, \ldots, \tilde{b}$. Numerically the front width is estimated by fitting a straight line, tangential to the inflection point $\rho(x^*) = g/2$, such as in Fig. 7, and the front width is approximated as the inverse slope of the fitted line.

Our analysis has shown that the front width depends directly on the front speed. As seen above in Eq. (36), the front speed v is determined by fitting numerically the parameter K. Eq. (39) suggests that the same K, used for the calculation of v, allows for the prediction of the front width W. This result can be easily confirmed numerically.

4. Discussion

Our focus was to establish a simple LGCA model of tumor invasion and to analyze the observed traveling front behavior. In the present study, we restrict our analysis to the characterization of the invading traveling front behavior in a homogeneous environment of two interacting populations of tumor cells and necrotic material. Via the cut-off mean-field analysis of the linearized discrete LBE, we derive a reaction–diffusion equation that describes our system macroscopically. This cut-off R-D equation enables us to calculate accurately the speed of the tumor wavefronts.

The simulations show a "layer" formation of cancer and necrotic cells which is observed in numerous experiments [23,33]. This behavior is a result of the tumor cell interactions. Mitosis creates an invasive tumor wavefront and the succeeding and increasing necrotic core follows the moving tumor border. Some experimental data suggest a linear growth kinetic for tumors [33]. Our simulations show that the growth behavior of our model is consistent with these experimental observations. We predict the front velocity to scale with the square root of the product of rates for mitosis and migration. This means that we are able to calculate the tumor invasion speed by incorporating experimentally accessible parameters, for example the mitotic rate and cell motility rate, respectively. The behavior of the front depends solely on the behavior of the tumor cells and not on the necrotic material. Another important aspect of the invasive behavior is the width of the front. It is of great interest that the estimation of the length of tumor's invasive zone which coincides with the width of the traveling front. In particular, the invasive zone is of vital importance for the tumor since the majority of mitotic activity is concentrated within this zone. Thus, it is important to develop mathematical tools that allow the estimation of the tumor's front width. Here, we provide an estimate of front width which is proportional to the speed of the tumor front.

A straightforward extension of the model is the consideration of the host's environment, as shown in [4]. Moreover, we can incorporate specific tumor cell dynamics, such as the so-called migration/proliferation dichotomy [34], and investigate the resulting tumor behavior. Finally, recent studies on the fractality of tumor surfaces [33] have shown that tumors belong to a specific universality class of growth. The present study sets the basis for the analysis of more realistic and complicated models.

Acknowledgements

We are grateful to A. Chauviere, F. Peruani and M. Tektonidis for fruitful discussions. Special thanks go to Elan Gin for proof-reading the English of our manuscript. We acknowledge support by the systems biology network HepatoSys of the German Ministry for Education and Research through grant 0313082J, and support by the Gottlieb Daimler- and Karl Benz-Foundation through their research program "From bio-inspired logistics to logistics-inspired bio-nano-engineering". Andreas Deutsch is a member of the DFG Research Center for Regenerative Therapies Dresden – Cluster of Excellence – and gratefully acknowledges the support by the Center. The research was supported in part by funds from the EU Marie Curie Network "Modeling, Mathematical Methods and Computer Simulation of Tumor Growth and Therapy" (EU-RTD IST-2001-38923).

Appendix

In this Appendix, we present the details of the micro-dynamical Eqs. (5) and (6). In the following for simplicity reasons and without any loss of generality, we drop the spatial and the temporal arguments of the functions. The Heaviside functions $\Theta(\theta_M - n_C)$ and $\Theta(n_C - \theta_N)$ can be alternatively written in terms of random variables:

$$\Theta(\theta_M - n_C) = \sum_{l=1}^{\theta_M} \delta(n_C = l) = \begin{cases} 1, & \text{if } n_C \leq \theta_M \\ 0, & \text{else} \end{cases} \tag{40}$$

$$\Theta(n_C - \theta_N) = \sum_{l=\theta_N}^{\tilde{b}} \delta(n_C = l) = \begin{cases} 1, & \text{if } n_C \geq \theta_N \\ 0, & \text{else} \end{cases} \tag{41}$$

where the $\delta(n_C)$ functions represent the possible node configurations that account for n_C number of cells, defined in the general form:

$$\delta(n = N) = \sum_{l=1}^{\binom{\tilde{b}}{N}} \prod_{i \in M_l^n} \eta_i(r,k) \prod_{j \in M/M_l^n} (1 - \eta_j(r,k)) = \begin{cases} 1, & \text{if } n = N \\ 0, & \text{else} \end{cases} \tag{42}$$

where $N \in \{0, \ldots, \tilde{b}\}$ and the index set $M = 1, \ldots, \tilde{b}$ and M_l^n denotes the nth subset of M with l elements. Using Eqs. (40)–(42) in combination with Eq. (5), (6), we can write the micro-dynamical equations in terms of occupation numbers.

Now let us evaluate the expected collision operators $\tilde{C}_{\sigma,i}$ from Eqs. (10) and (11). We assume that $\theta_M = 4$ and $\theta_N = 6$ and that the system is in the steady state $(\bar{f}_C, \bar{f}_N)$. Moreover, we fix the node capacity as $\tilde{b} = 4$. Therefore, Eqs. (10) and (11) yield:

$$\begin{aligned} \tilde{C}_{C,i} = \frac{1}{8}\Big[& r_M\big(\bar{f}_C(1-\bar{f}_C)^7 + 28\bar{f}_C^2(1-\bar{f}_C)^6 + 56\bar{f}_C^3(1-\bar{f}_C)^5 + 70\bar{f}_C^4(1-\bar{f}_C)^4\big) \\ & - r_N\big(28\bar{f}_C^6(1-\bar{f}_C)^2 + 8\bar{f}_C^7(1-\bar{f}_C)^1 + \bar{f}_C^8\big)\Big], \end{aligned} \tag{43}$$

$$\tilde{C}_{N,i} = \frac{1}{8}\Big[r_N(1-\bar{f}_N)\big(28\bar{f}_C^6(1-\bar{f}_C)^2 + 8\bar{f}_C^7(1-\bar{f}_C)^1 + \bar{f}_C^8\big)\Big]. \tag{44}$$

Setting $\tilde{C}_{\sigma,i} = 0$, we can calculate the exact values of the steady states $(\bar{f}_C, \bar{f}_N)$ in (12).

References

[1] P.C. Nowell, The clonal evolution of tumor cell populations, Science 194 (4260) (1976) 23–28.
[2] D. Hanahan, R. Weinberg, The hallmarks of cancer, Cell 100 (2000) 57–70.
[3] P. Friedl, Prespecification and plasticity: Shifting mechanisms of cell migration, Curr. Opin. Cell. Biol. 16 (1) (2004) 14–23.
[4] H. Hatzikirou, A. Deutsch, Cellular automata as microscopic models of cell migration in heterogeneous environments, Curr. Top. Dev. Biol. 81 (2008) 401–434.
[5] M. Marusic, Z. Bajzer, J.P. Freyer, S. Vuk-Pavlovic, Analysis of growth of multicellular tumor spheroids by mathematical models, Cell Prolif. 27 (1994) 73–94.
[6] A.R. Kansal, S. Torquato, G.R. Harsh IV, E.A. Chiocca, T.S. Deisboeck, Simulated brain tumor growth dynamics using a three-dimensional cellular automaton, J. Theoret. Biol. 203 (2000) 367–382.
[7] B.P. Marchant, J. Norbury, A.J. Perumpanani, Traveling shock waves arising in a model of malignant invasion, SIAM. J. Appl. Math. 60 (2) (2000) 263–276.
[8] A.J. Perumpanani, J.A. Sherratt, J. Norbury, H.M. Byrne, Biological inferences from a mathematical model of malignant invasion, Invasion. Metastasis. 16 (1996) 209–221.
[9] A.J. Perumpanani, J.A. Sherratt, J. Norbury, H.M. Byrne, A two parameter family of traveling waves with a singular barrier arising from the modelling of extracellular matrix mediated cellular invasion, Physica D 126 (1999) 145–159.
[10] J.A. Sherratt, M.A. Nowak, Oncogenes, anti-oncogenes and the immune response to cancer: A mathematical model, Proc. Roy. Soc. Lond. B 248 (1992) 261–271.

[11] J.A. Sherratt, M.A.J. Chaplain, A new mathematical model for avascular tumor growth, J. Math. Biol. 43 (2001) 291–312.
[12] P. Tracqui, G.C. Cruywagen, D.E. Woodward, G.T. Bartoo, J.D. Murray, E.C. Alvord Jr, A mathematical model of glioma growth: The effect of chemotherapy on spatio-temporal growth, Cell Prolif. 28 (1995) 17–31.
[13] K.R. Swanson, E.C. Alvord Jr, J.D. Murray, Quantifying efficacy of chemotherapy of brain tumors (gliomas) with homogeneous and heterogeneous drug delivery, Acta Biotheor. 50 (2002) 223–237.
[14] H.B. Frieboes, S. Wise, X. Zheng, P. Macklin, E. Bearer, V. Cristini, Computer simulation of glioma growth and morphology, Neuroimage 37 (2007) 59–70.
[15] H. Hatzikirou, A. Deutsch, Cellular automata models of tumor invasion, Encyclopedia of Complexity and Systems Science, Springer, Heidelberg 2009 (in press).
[16] A. Deutsch, S. Dormann, Cellular Automaton Modeling of Biological Pattern Formation, Birkhäuser, Boston, 2005.
[17] U. Frisch, D. d'Humieres, B. Hasslacher, P. Lallemand, Y. Pomeau, J.P. Rivet, Lattice gas hydrodynamics in two and three dimensions, Compl. Syst. 1 (1987) 649–707.
[18] S. Dormann, A. Deutsch, Modeling of self-organized avascular tumor growth with a hybrid cellular automaton, Sil. Biol. 2 (2002) 0035.
[19] M. Wurzel, C. Schaller, M. Simon, A. Deutsch, Cancer cell invasion of normal brain tissue: Guided by prepattern? J. Theoret. Med. 6 (1) (2005) 21–31.
[20] D. Wolf-Gladrow, Lattice-Gas Cellular Automata and Lattice Boltzmann Models: An Introduction, Springer, New York, 2000.
[21] B. Chopard, M. Droz, Cellular Automata Modeling of Physical Systems, Cambridge University Press, Cambridge, 1998.
[22] D. Dab, J. Boon, Y.X. Li, Lattice-gas for coupled reaction-diffusion equations, Phys. Rev. Lett. 66 (1991) 2535–2538.
[23] J. Folkman, M. Hochberg, Self-Regulation of growth in three dimensions, J. Exp. Med. 138 (1973) 745–753.
[24] J.P. Boon, D. Dab, R. Kapral, A. Lawniczak, Lattice gas automata for reactive systems, Phys. Rep. 273 (1996) 55–148.
[25] K. Tucci, R. Kapral, Mesoscopic multiparticle collision model for reaction-diffusion fronts, J. Phys. Chem. B 109 (2005) 21300.
[26] H.P. Breuer, W. Huber, F. Petruccione, Fluctuation effects on wave propagation in a reaction–diffusion process, Physica D 73 (1994) 259.
[27] M.V. Velikanov, R. Kapral, Fluctuation effects on quadratic autocatalysis fronts, J. Chem. Phys. 110 (1999) 109–115.
[28] I. Brunet, B. Derrida, Shift in the velocity of a front due to a cutoff, Phys. Rev. E 56 (3) (1997) 2597–2604.
[29] E. Cohen, D. Kessler, H. Levine, Fluctuation-regularized front propagation dynamics in reaction-diffusion systems, Phys. Rev. Lett. 94 (2005) 158302.
[30] R.D. Benguria, M.C. Depassier, V. Mendez, Propagation of fronts of a reaction-convection-diffusion equation, Phys. Rev. E 69 (2004) 031106(7).
[31] J. Murray, Mathematical Biology I: An Introduction, Spinger, 2001.
[32] I. Brunet, B. Derrida, Effect of microscopic noise in front propagation, J. Stat. Phys. 103 (1/2) (2001) 269–282.
[33] A. Bru, S. Albertos, J.L. Subiza, J. Lopez Garcia-Asenjo, I. Bru, The universal dynamics of tumor growth, Biophys. J. 85 (2003) 2948–2961.
[34] H Hatzikirou, B. Basanta, M. Simon, C. Schaller, A. Deutsch, Go or Grow: The key to the emergence of invasion in tumor progression? (in press).